GEOPHYSICS, VOL. 64, NO. 4 (JULY-AUGUST 1999); P. 1266–1276, 14 FIGS.

Fracture detection in a carbonate reservoir using a variety of seismic methods

Maria A. Pérez*, Vladimir Grechka‡, and Reinaldo J. Michelena*

ABSTRACT

We combine various methods to estimate fracture orientation in a carbonate reservoir located in southwest Venezuela. The methods we apply include the 2-D rotation analysis of 2-D *P-S* data along three different azimuths, amplitude-variation-with-offset (AVO) of 2-D *P*-wave data along the same three azimuths, normal-moveout (NMO) analysis of the same 2-D data, and both 3-D azimuthal AVO and NMO analysis of 3-D *P*-wave data recorded in the same field.

The results of all methods are compared against measures of fracture orientation obtained from Formation microScanner logs recorded at four different locations in the field, regional and local measures of maximum horizontal stress, and the alignment of the major faults that cross the field.

P-S data yield fracture orientations that follow the regional trend of the maximum horizontal stress, and are consistent with fracture orientations measured in the wells around the carbonate reservoir. Azimuthal AVO analysis yields a similar regional trend as that obtained from the *P-S* data, but the resolution is lower. Local variations in fracture orientation derived from 3-D AVO show good correlation with local structural changes. In contrast, due to the influence of a variety of factors, including azimuthal anisotropy and lateral heterogeneity in the overburden, azimuthal NMO analysis over the 3-D *P*-wave data yields different orientations compared to those obtained by other methods. It is too early to say which particular method is more appropriate and reliable for fracture characterization. The answer will depend on factors that range from local geological conditions to additional costs for acquiring new information.

INTRODUCTION

Fracture characterization is an important part of reservoir development, in particular for carbonate reservoirs. Different techniques have been used to estimate fracture orientation and density. Traditionally, *S*-waves generated at the surface and recorded by three component geophones (either with vertical seismic profiling or surface geometries) have been used for this purpose (Alford, 1986). However, since acquisition and processing of *S*-waves is costly and the availability of shear waves sources is limited, different alternatives have been considered.

Recently, *P-S* converted waves have become more popular because they are expected to contain the same information as *S-S* waves but can be generated with compressional sources, which makes the acquisition not only inexpensive but also less labor intensive than *S-S* waves recording. Garotta and Granger (1988) and Ata and Michelena (1995) showed examples of the use of *P-S* converted waves to estimate fracture orientation. *P-S* waves, however, are more cumbersome to use than non-converted waves because of the asymmetry of the ray path, and they are more expensive to record and process than conventional *P-P* waves.

Since many areas in the world are already covered by 3-D *P*-wave data, various authors have focused their attention on the use of this existing information to estimate fracture properties. A modeling exercise presented by Mallick and Frazer (1991) shows that the amplitude-variation-with-offset (AVO) response of *P*-waves can be affected by the presence of fractures depending on the relative orientation between fractures and the recording line. Lefeuvre (1994), Lynn et al. (1995), Pérez and Gibson (1996), and Pérez et al. (1999) presented examples that confirmed Mallick and Frazer's (1991) predictions. Rüger (1996) developed the theory behind these observations and showed how to estimate other fracture properties besides orientation.

A more recent line of research initiated by Grechka and Tsvankin (1996) is devoted to the estimation of fracture

Manuscript received by the Editor February 24, 1998; revised manuscript received January 19, 1999.
*PDVSA-Intevep, Aptdo 76343, Caracas 1070A, Venezuela. E-mail: maru@intevep.pdv.com; michelen@intevep.pdv.com.
‡Center for Wave Phenomena, Dept. of Geophysics, Colorado School of Mines, Golden, Colorado 80401. E-mail: vgrechka@dix.mines.edu.

properties from the normal-moveout (NMO) analysis of multiazimuth *P*-wave data. Corrigan et al. (1996) successfully applied these ideas to field data.

All the previously mentioned methods have their own limitations and do not necessarily yield the same results when applied in the same area. They are influenced by different sources of noise that need to be properly considered and reduced to obtain accurate results.

In this study, we compare the results of different seismic methods used to estimate fracture orientation when applied to different data sets recorded in the same field. The methods we use are the rotational analysis of converted waves, azimuthal AVO analysis, and NMO ellipticity. The results obtained from different methods generally agree (except that for 3-D NMO ellipticity), follow one of the fracture sets detected with Formation microScanners (FMS) logs, and coincide with the trend of the maximum horizontal stress in the area.

THE STUDY AREA

Maporal field is located in the north-central part of the Barinas-Apure Basin, near the Andes, in Venezuela. Structurally, Maporal field is a dome slightly extended toward the northeast. Geologically, the sediments are nearly flat-lying, dipping toward the northeast at approximately 4°. The target zone is the "O" member of the Escandalosa Formation. This member is a 25-m-thick fractured limestone located at a depth of approximately 3000 m (2.32 s). Since fractures seem to control production from the Escandalosa Formation, reservoir engineers decided to continue the exploitation of the field using horizontal wells oriented perpendicularly to the densest fracture systems. Seismic data were recorded to help engineers achieve their goal.

Existing well log information in the field provides good background information about the reservoir and its fracture properties, and can be used to calibrate the results obtained from the seismic data. Well data include gamma-ray, resistivity, and dipole sonic logs, which provided information about *P*- and *S*-waves around the target. FMS logs were used to estimate fracture orientation, fracture density, and orientation of maximum horizontal stress at four different wells. The rose diagrams in Figure 1 shows the presence of different fracture systems in the area. However, the orientation of the maximum horizontal stress measured in the same wells is constant across the field. The open fracture system tends to be the one parallel or quasi-parallel to the orientation of maximum horizontal stress.

AVAILABLE DATA

The data sets used for this study consisted of a 3-D *P*-wave survey recorded over an area (640 km^2) much larger than the area of interest to help in the characterization of other adjacent reservoirs, and three 10-km 2-D 3-C lines centered in the area of interest (Figure 2). The multicomponent acquisition was performed right after the 3-D acquisition finished and, therefore, the results of the analysis of one data set were not used to help the design of the other.

The three 2-D 3-C multicomponent lines were centered over the area of interest with an intersection point coinciding with a well location. For calibration purposes, each line intersected, or was close to, at least one additional well with log information. Previous *P*-wave 2-D seismic data were used to identify two nearly orthogonal faults systems that cross the field (Figure 1). The azimuths of two of the multicomponent lines were almost parallel to these systems, whereas the other line bisected them, forming an angle of approximately 45° with each. A noise-

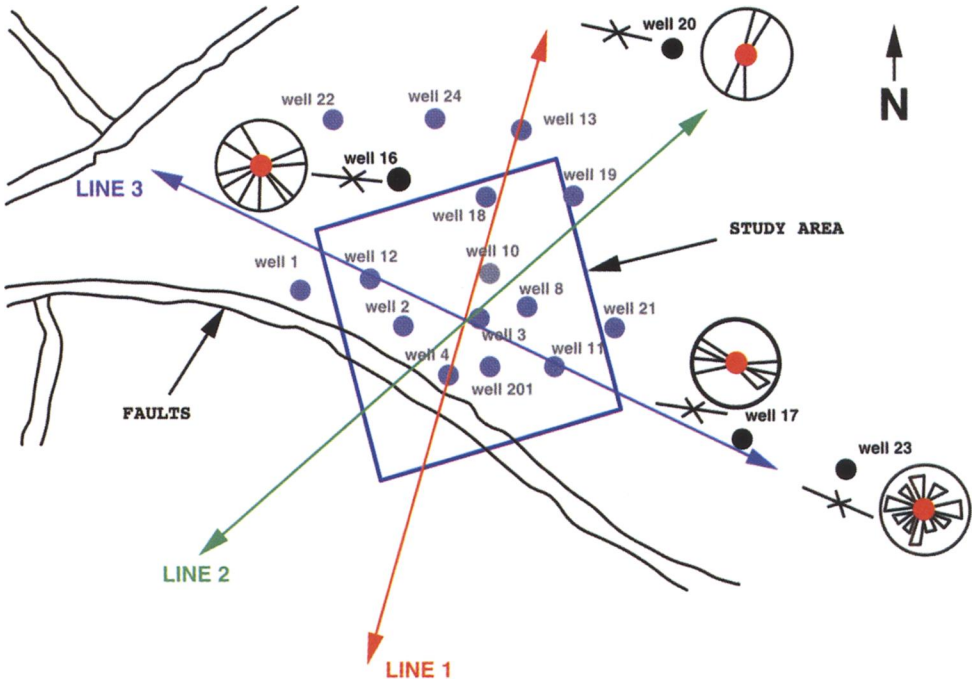

FIG. 1. Maximum horizontal stress (inward facing arrows) from break-out orientation logs at wells 16, 17, 20, and 23. The rose diagrams indicate fracture orientation and density from FMS logs in the same wells.

spread test was used to optimize the design and enhance the quality of the converted waves.

The 3-D seismic data were collected using a swath geometry with a shot line perpendicular to eight receivers lines. A bin spacing of 80 m, a fold of approximately 40 traces, and a maximum offset of 3626 m were acquired. A subset of 25 km^2 from the original 3-D data set centered at the intersection point of the 2-D multicomponent lines was used for this study. Superbins of 240 × 240 m^2 were formed to insure adequate coverage in offset and azimuth for AVO and NMO analysis.

The processing sequence of both data sets was designed to preserve relative amplitude, maximize frequency band, and optimize velocity analyses for all components. Refraction statics estimated from a *P*-wave refraction survey were applied to both 2-D and 3-D data. Converted wave statics in the 2-D 3-C data were corrected by using *P*-wave statics and various iterations of residual statics. Figure 3 shows a typical CDP supergather from the 3-D data. Only *f-k* filtering in the shot domain has been applied to these data to eliminate surface waves. Notice how the presence of static noise, or possible azimuthal anisotropy,

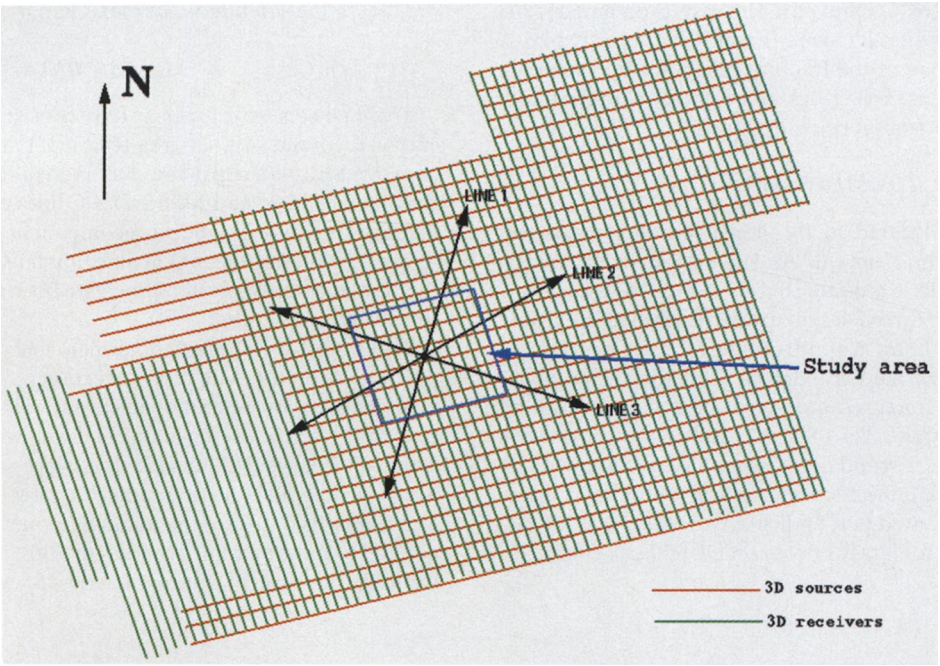

FIG. 2. Study area over 2-D and 3-D surveys.

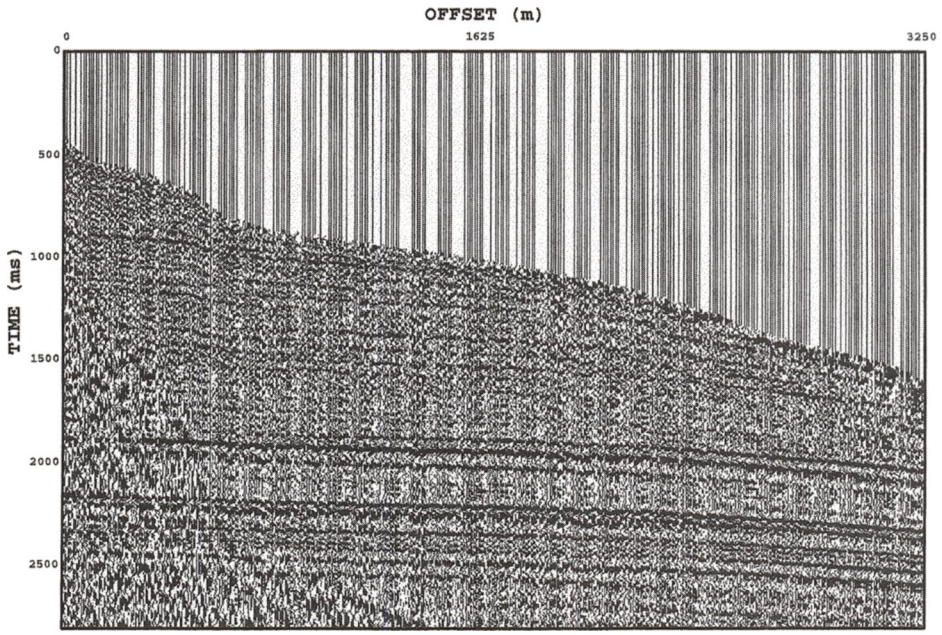

FIG. 3. Typical supergather from 3-D data. The bin size is 240 × 240 m^2.

influences the continuity of all reflections. Reflections from the top of the target (Escandalosa Formation) are located at 2.32 s. Figure 4 shows a 2-D 3C, raw common-shot gather recorded over line 2. Notice the presence of energy in both horizontal components, which is an indication of azimuthal anisotropy. Michelena et al. (1994) performed modeling to demonstrate that azimuthal anisotropy, not heterogeneity, is responsible for the energy observed in the transverse component in this area. As shown by Ata and Michelena (1995), fracture orientation changes across the field, which explains why not all 3-C records show energy in the transverse component. Converted waves from the top of Escandalosa Formation are indicated by the arrow at 3.8 s.

Figure 5 shows the structural map of the top of the Escandalosa Formation interpreted from the 3-D *P*-wave seismic data. This map confirms the gentle nature of the structural variations in the field already known from previous 2-D *P*-wave data. As we mentioned before, this structure dips 4° toward the northeast.

DATA ANALYSIS

We estimate fracture orientation by applying different methods to the different data sets available. We start by analyzing the *P-S* converted waves in the multicomponent data. Then, we analyze the AVO and NMO responses of *P*-waves recorded in the vertical component of the 2-D 3-C data around the intersection point of the three lines. Finally, we examine the azimuthal variations of AVO and NMO responses of the *P*-waves for each bin in the 3-D data. This section describes these results.

2-D data

Rotation analysis of *P-S* converted waves.—Figure 6 shows portions of migrated horizontal components around three different points in the field. Notice that points located on lines 1 and 3 clearly show that the horizontal component parallel to line 3 arrives earlier than the other component, which is what we expected from the direction of the maximum horizontal stress in the field. Remember that the orientation of the faster shear arrival generally coincides with the direction of maximum horizontal stress.

After interpreting the migrated sections of radial and transverse components, we compute rms amplitudes in a window around the target. Then, we perform rotational analysis based on the amplitude ratio between the two horizontal components (Ata and Michelena, 1995) to estimate fracture orientation for each common conversion point (CCP) of the three lines. From the angles estimated at each CCP, we obtain new angles for points outside the multicomponent lines using 2-D spline interpolation. The orientation of the fastest shear arrival happens to be approximately constant for all depths across the field.

Figure 7 shows a smoothed map with the results of the rotational analysis plus interpolation. Each arrow indicates the local fracture orientation (fracture strike) estimated from converted waves. The colors show the same structural map presented in Figure 5. Since the azimuths between the lines have been interpolated, orientations presented in this map are more reliable along and in the neighborhood of the three lines. As we can see, fracture orientation follows the trend of the maximum horizontal stress in the area. Notice that the estimated fracture orientation follows the direction of one of the fracture systems present in the area.

Azimuthal AVO from 2-D data.—For the 2-D *P*-wave data, we perform conventional AVO analysis over CDP gathers located along each line close to the intersection point. We obtain the sections of AVO gradient and AVO intercept for each line. Figure 8 shows the AVO gradient sections around the

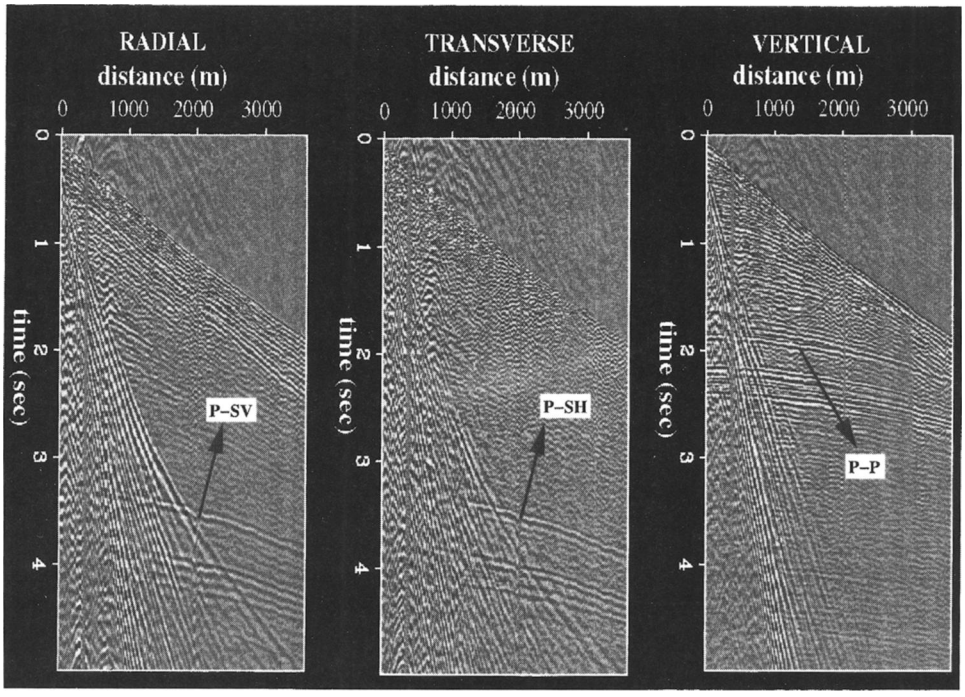

FIG. 4. 3-C raw common-shot gather recorded over line 2 of the 2-D multicomponent lines. Converted waves from the top of Escandalosa Formation are indicated by the arrow at 3.8 s in the horizontal components.

intersection point along almost perpendicular lines 1 and 3. Notice the different AVO gradients for the reflection from the bottom of the reservoir along these two lines. No significant differences are observed in AVO response from the top of the reservoir. Figure 9 is a graph of AVO gradient versus AVO intercept. Gradients for lines 1 and 2 (nearly perpendicular to fracture orientation) are positive and higher than gradients along line 3 (which is nearly parallel to the fracture orientation

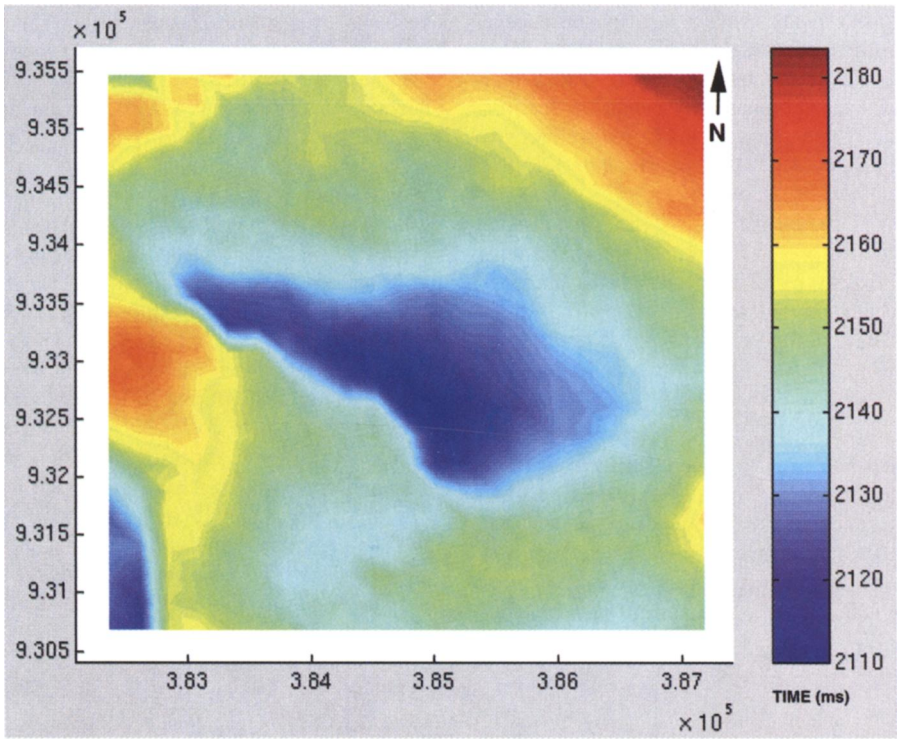

FIG. 5. Structural map of the top of Escandalosa Formation interpreted from the 3-D seismic data. Colors indicate two-way traveltime in seconds.

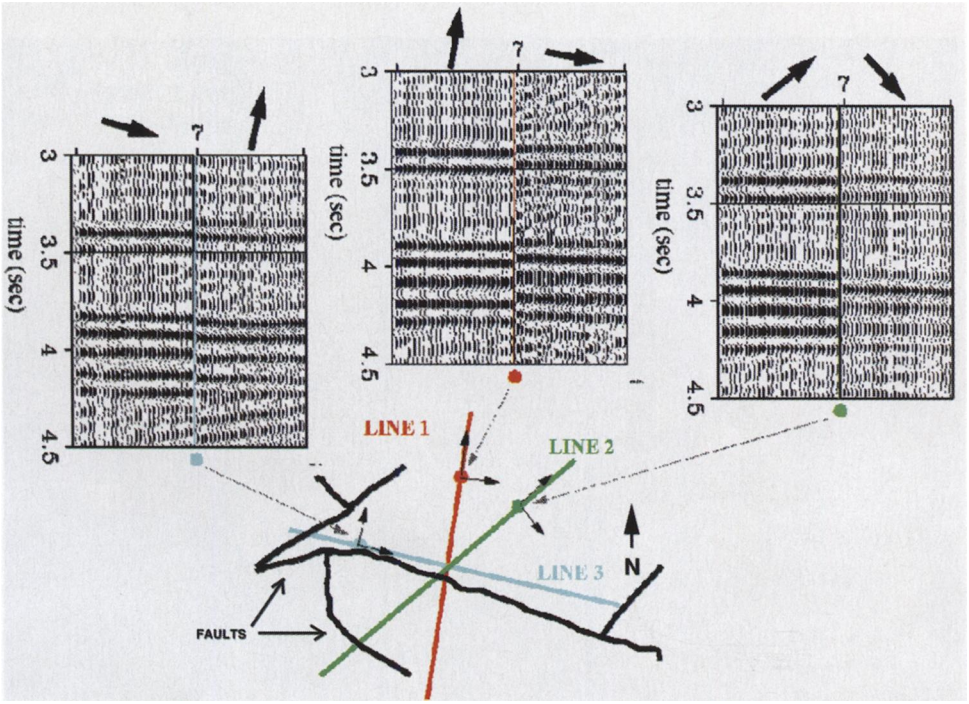

FIG. 6. Horizontal components from three different locations in the field.

estimated from converted waves). As expected, the AVO intercept is almost the same for all lines. This result is consistent with the observations of Mallick and Frazer (1991) and Johnson (1995) that, in the presence of azimuthal anisotropy, AVO characteristics along different shooting directions are similar for near-normal reflections and may differ for wide-angle reflections.

The exact direction of the maximum AVO gradient was estimated from the three CDP gathers located at the intersection point of the multicomponent lines. We use a formula derived by Rüger (1996) for the reflection coefficients in transversely isotropic media with a horizontal symmetry axis. The estimated azimuth of the maximum AVO gradient is 56°. Since it is expected to be perpendicular to fracture orientation, we obtain the fracture azimuth as 146° (Figure 10). As we can see, fracture orientation estimated using this technique also follows the regional maximum horizontal stress and is close to the orientation obtained from the analysis of the converted waves (Figure 7).

NMO ellipticity from 2-D data.—From the same three gathers used to obtain the orientation of the maximum AVO gradient, we estimate the parameters that describe the best-fitting horizontal ellipse of the NMO velocities for all azimuths (Grechka and Tsvankin, 1996). The NMO ellipse obtained from this analysis is shown in Figure 11. The azimuth of the major axis is 125°. The major axis corresponds to the maximum NMO velocity that is expected to coincide with fracture orientation. The differences between maximum and minimum velocities are around 5%, but the axes of the ellipse have been exaggerated to give a better idea of its orientation. In this case, the orientation of the major axis of the NMO ellipse also follows the regional trend of the maximum horizontal stress in the area.

3-D data

Azimuthal AVO from 3-D data.—3-D *P*-wave data was gathered using a bin size of 240 × 240 m^2 to achieve the coverage needed in both offset and azimuth to perform azimuthal AVO analysis. The orientation of the maximum AVO gradient was estimated for each superbin based on the amplitudes located within a time window that follows the structural interpretation of the top of Escandalosa Formation (Figure 5).

Figure 12 shows smoothed results of the azimuthal AVO analysis for each superbin. The arrows in Figure 12 are oriented according to these new, smoothed angles. As we can see, the estimated orientations follow closely the local structural changes, but the general trend is still close to the regional maximum horizontal stress. Areas with abrupt changes in structure seem to have a more erratic AVO response when compared to other areas in the field.

Notice the similarity between the results obtained with converted waves (Figure 7) and 3-D azimuthal AVO analysis (Figure 12). There are differences, however, between the two results, especially in the northwest part of the area. No interpolation was used to generate Figure 12 because AVO analysis was performed at equally spaced grid points. On the contrary, to generate Figure 7, we interpolated the azimuths measured along the lines for all grid points where no information was available. In principle, this can create unrealistic orientations in areas surrounded by angles that represent the same direction but different orientations (0° and 180°, for instance), which is the case in the northwest part of the area. No attempt was made to change these angles in the data before interpolation.

NMO ellipticity from 3-D data.—3-D NMO analysis was performed for the same superbins used in the 3-D azimuthal AVO

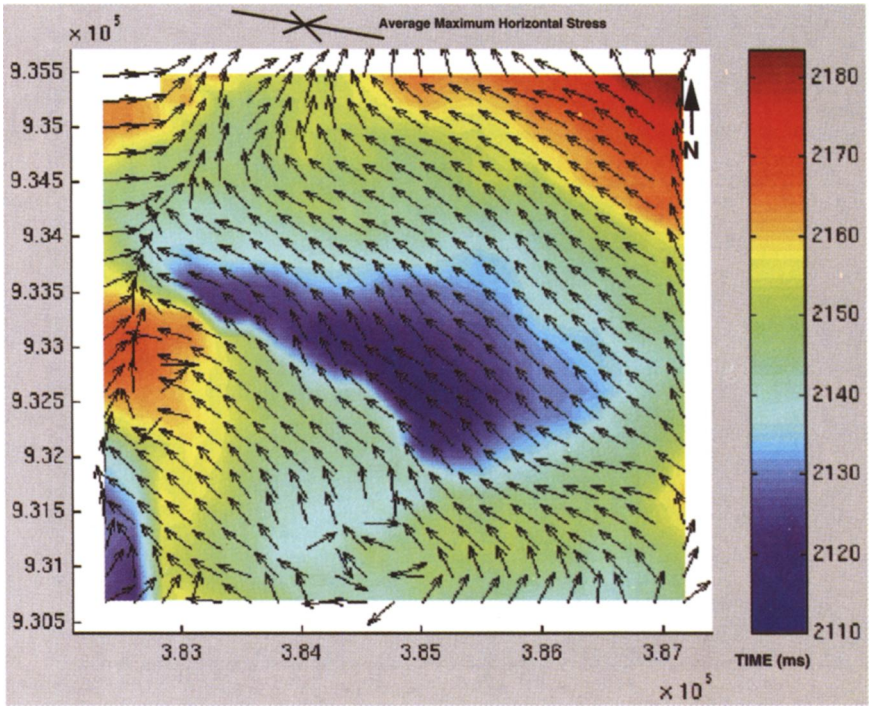

FIG. 7. Fracture orientation from rotational analysis of converted waves.

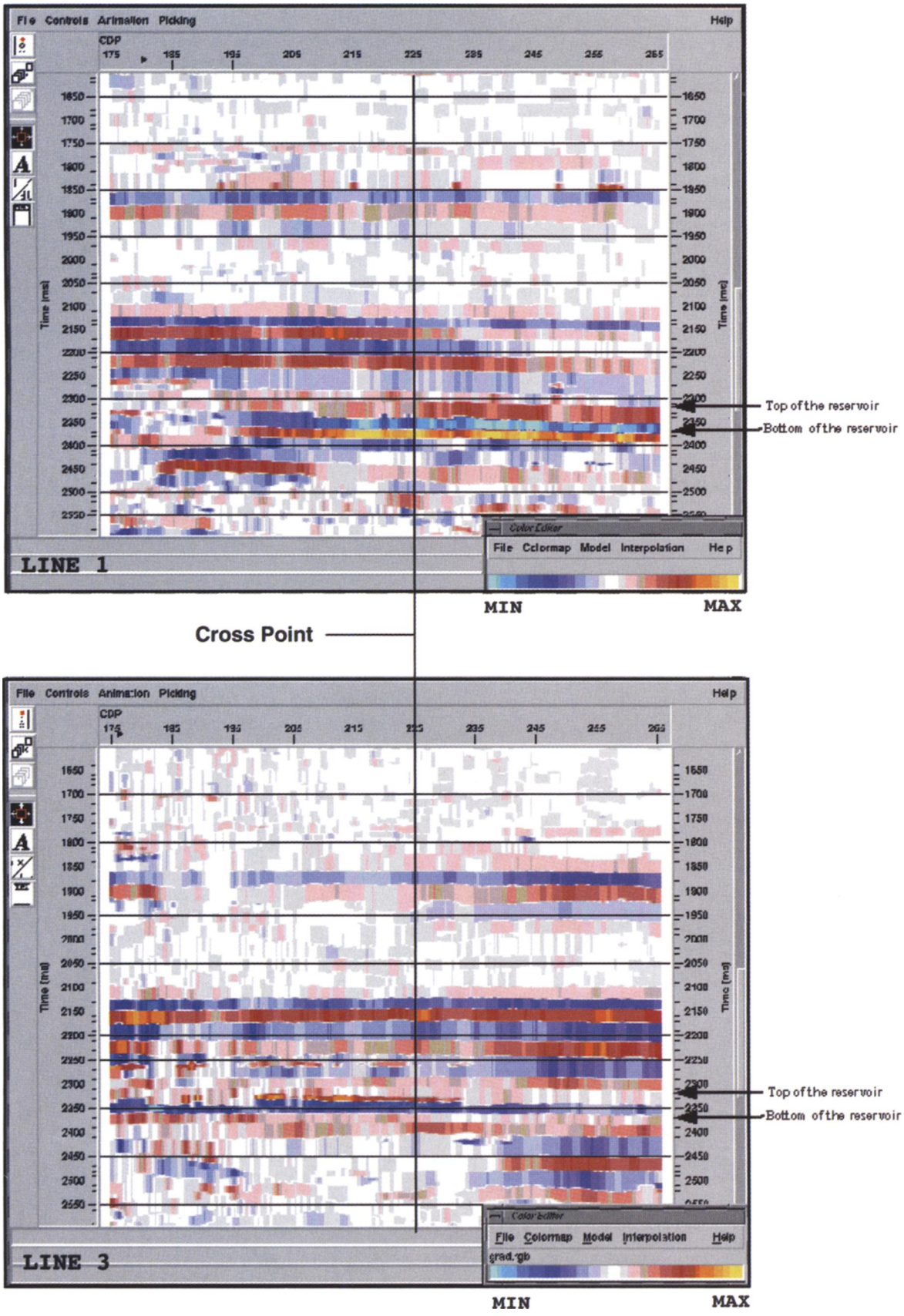

FIG. 8. AVO gradient sections around the interception point for lines 1 and 3. Notice how the AVO response changes around the bottom of the reservoir located at 2.370 s.

analysis. Figure 13 shows the result of this process: the orientation of the semimajor axes of NMO ellipses at the target for each CDP. The general trend in the orientation of these axes is not as expected from all our previous results, which followed the orientation of the maximum horizontal stress more closely. In Figure 13, the differences between the semimajor and semiminor axes of the NMO ellipse are of the order of 3%.

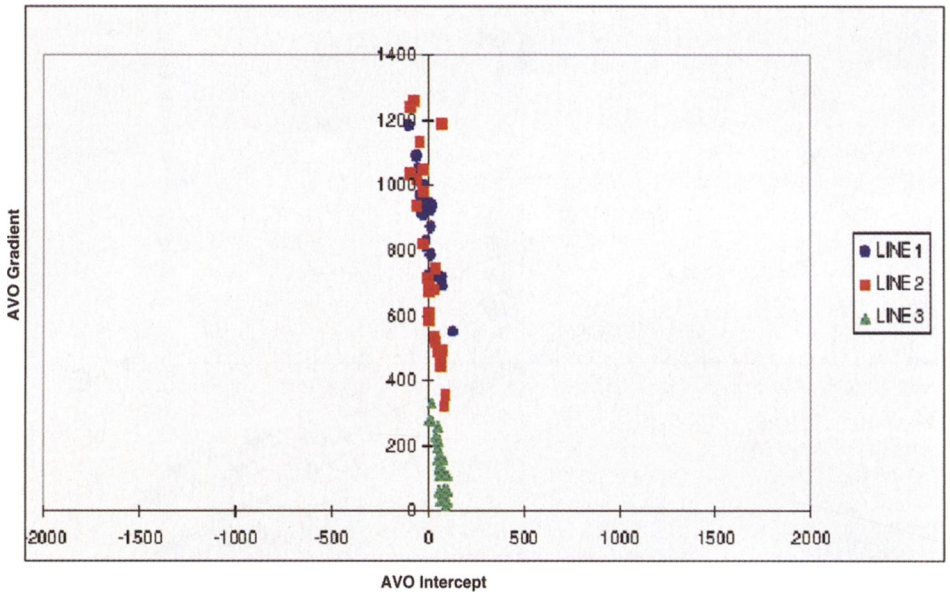

FIG. 9. AVO intercept versus AVO gradient for lines 1, 2, and 3 at the intersection point of the 2-D multicomponent lines.

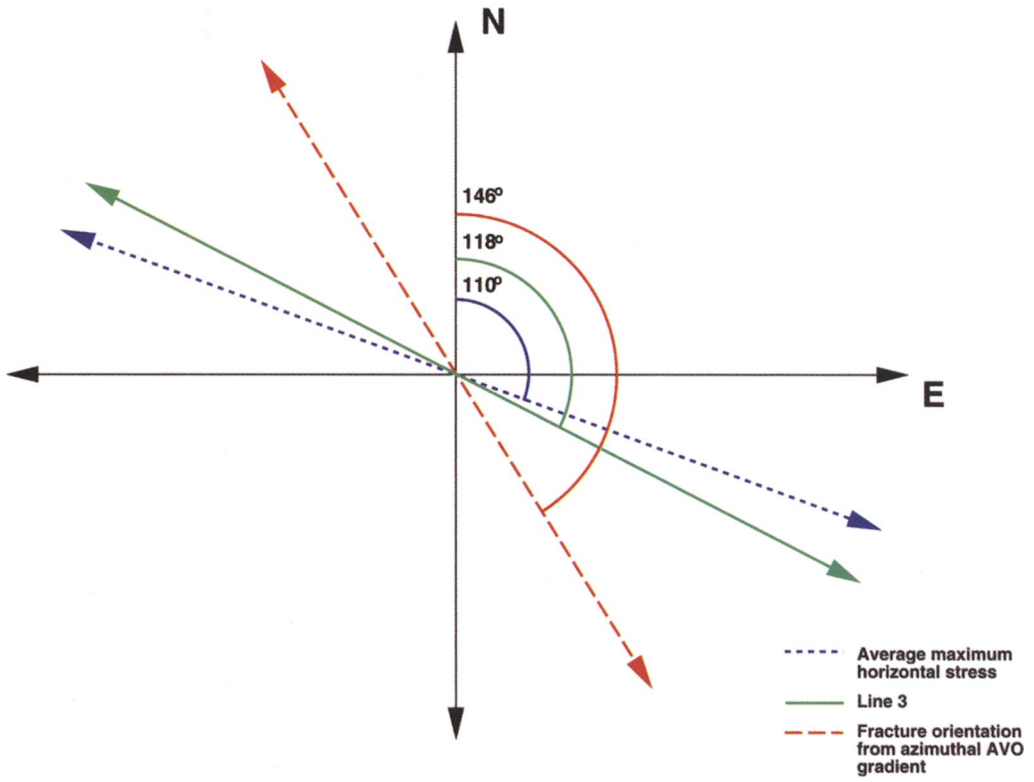

FIG. 10. Orientation perpendicular to the maximum AVO gradient at the intersection point of the 2-D multicomponent lines. This result is compared to the orientation of line 3, which is nearly parallel to the orientation of maximum horizontal stress in the area.

We can speculate about various reasons to explain the orientations of NMO ellipses for each CDP. First, the NMO ellipses include a cumulative influence of the overburden from the surface to the target. We did not do layer stripping to obtain interval velocities because the target is too thin (25 m) compared to its depth and, therefore, the error amplification due to stripping is expected to be severe. Second, since the ellipticities (i.e., the elongations of NMO ellipses) are small (about 3%),

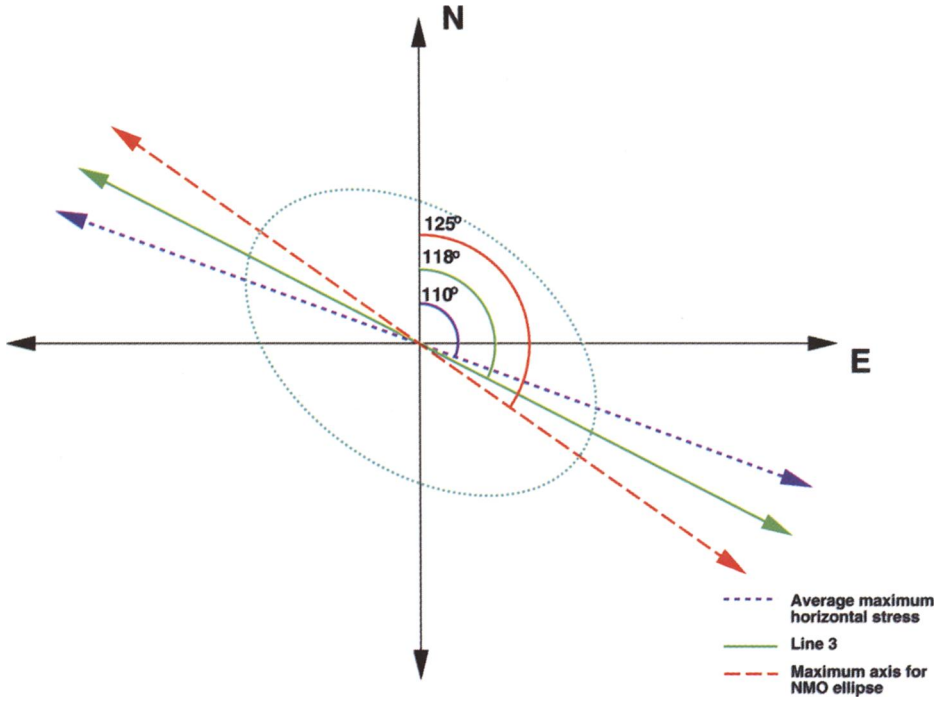

FIG. 11. Orientation of the NMO ellipse from 2-D *P*-wave data at the intersection point of the 2-D multicomponent lines.

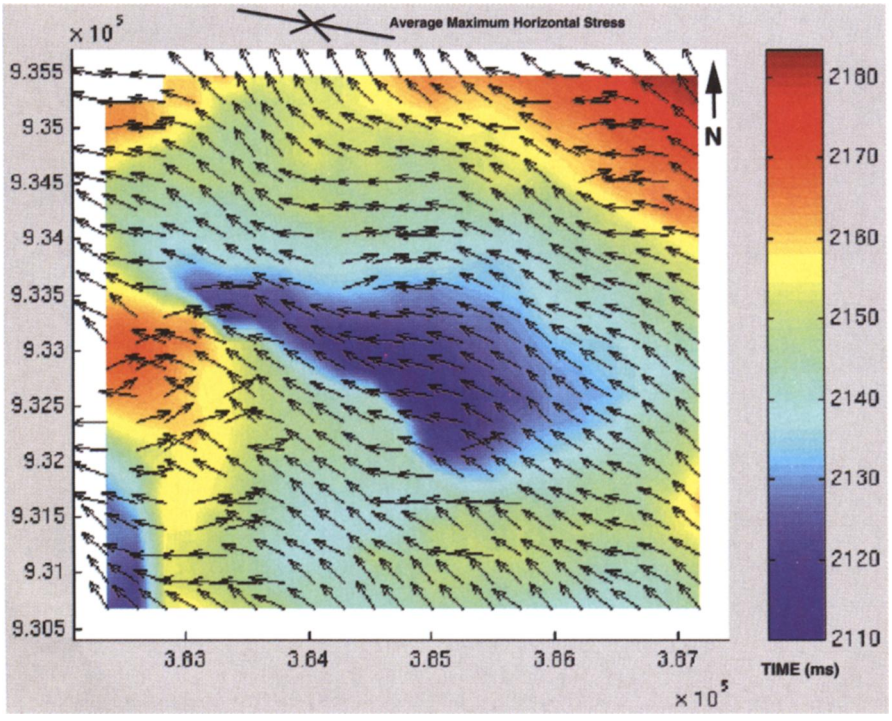

FIG. 12. Fracture orientation from 3-D azimuthal AVO analysis. The arrows indicate the local orientation of the perpendicular to the maximum AVO gradient.

the ellipse orientation becomes a poorly determined quantity, so that the estimated ellipse azimuths may be inaccurate. The third issue is that we believe that the proper way to remove the effects of near-surface azimuthal anisotropy is by doing independent static corrections for each azimuth, which we did only for the 2-D data. The effect of static variations, near-surface anisotropy, and azimuthal anisotropy in the subsurface that affect the NMO velocities cannot be separated with static correction methods that analyze simultaneously all azimuths in a superbin. We found that after applying such corrections for any

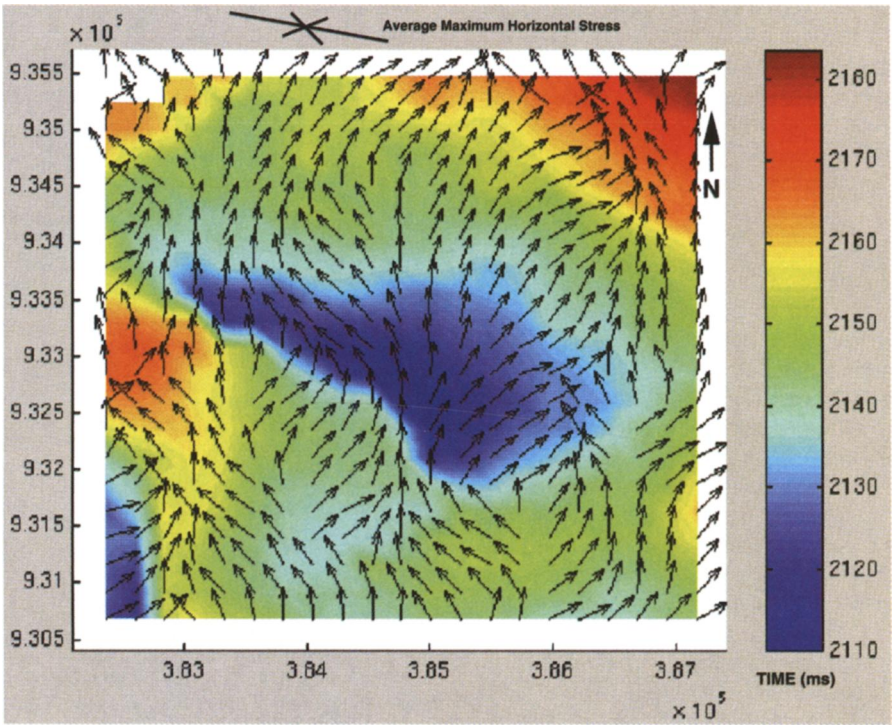

FIG. 13. Fracture orientation from 3-D NMO ellipticity. The arrows indicate the local orientation of the maximum axis for the NMO ellipse.

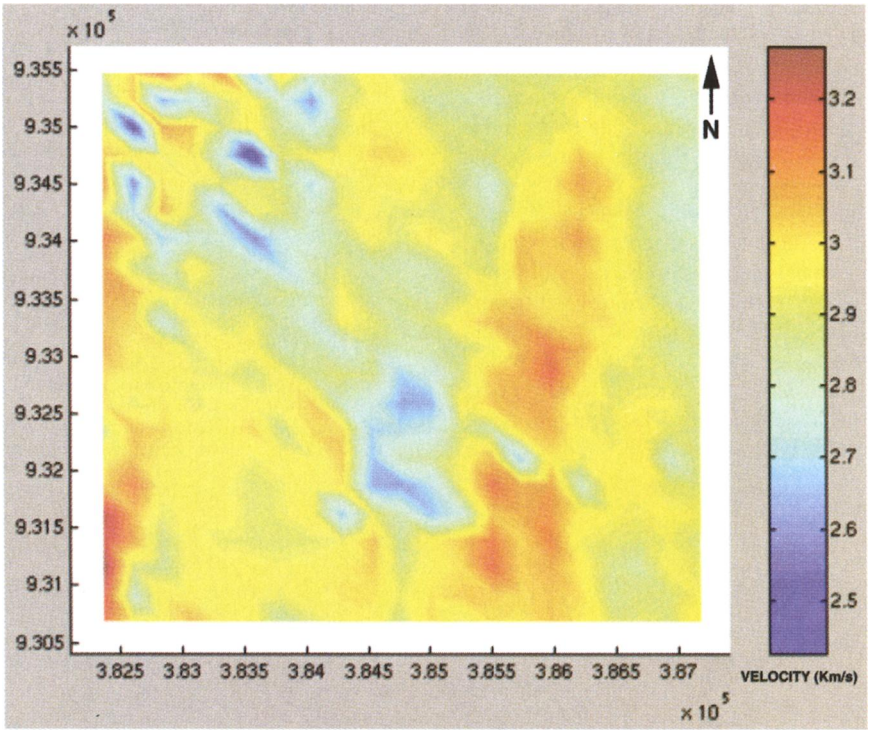

FIG. 14. Lateral velocity variations of the isotropic NMO velocity at the bottom of the reservoir.

depth, lateral coherency of events was improved considerably, but differences between major and minor axes of NMO ellipses were reduced to less than 0.01%. For this reason, we did not remove static corrections in the data used to generate Figure 13. Finally, the influence of lateral heterogeneity may make azimuthal variation of the NMO velocity elliptical even in the absence of anisotropy. Figure 14 shows lateral variations of the isotropic NMO velocity (e.g., a circular approximation of NMO ellipse) estimated from conventional velocity analysis around the target. Even though the changes in these velocities are not that large, they may distort our inferences about *P*-wave azimuthal anisotropy which are made under the assumption that the medium is laterally homogeneous.

CONCLUSIONS

We have applied a variety of methods to estimate fracture orientation using different kinds of surface seismic data recorded over the same reservoir. Most of the results from different methods (rotation analysis of *P-S*-wave 2-D data, and azimuthal AVO and NMO analysis of 2-D and 3-D *P*-wave data) captured the regional orientation of maximum horizontal stress in the field; however, when compared locally, the different methods may yield somewhat different answers. Local changes seem to be controlled by structural variations across the field. Even though the reservoir has several fracture systems, most of the applied methods picked the one that is closer to the orientation of the maximum horizontal stress.

The NMO ellipticity analysis over the 3-D data produced results different than those produced by other methods. Although several reasons may explain such differences, we believe that the most important ones include near-surface azimuthal anisotropy and overburden effects that could not be removed, and lateral velocity variations that may affect the estimated orientations. We believe static corrections should be performed independently for different azimuth ranges instead of correcting for all azimuths simultaneously. By doing azimuthally independent static corrections, we will avoid eliminating the effects of anisotropy in the subsurface that can be treated as near-surface variations if all azimuths are treated at once.

The answer to the question of whether there is a most appropriate and reliable method of fracture characterization depends on a variety of issues that need to be carefully analyzed. Ideally, if we have the resources to acquire multicomponent data, we should use this option that has proven its effectiveness in estimating not only fracture orientation but also fracture density. If we have only 3-D *P*-wave data with good amplitude control, our results suggest that 3-D azimuthal AVO analysis is more robust than 3-D azimuthal NMO analysis. If we have only 2-D *P*-wave data recorded along intersecting lines, we can use the results of azimuthal AVO and NMO analysis at the intersection points to obtain a low-resolution estimate of the fracture orientation. Such orientation may help to design further 3-D *P*-wave or multicomponent seismic acquisitions that yield higher resolution estimates.

In any case, we advise always using independent information that may be available from cores, well logs, and geology to assess the reliability of the results obtained with any particular method before drawing any final conclusions.

ACKNOWLEDGMENTS

We thank PDVSA-Intevep for permission to publish this work. We also thank Luis Lugo, Hector Pineda, and Elias Ata for their help in processing the data. We thank Ken Craft, Richard VanDok, and Gerard Beaudoin for their comments and suggestions that helped to improve the quality of this manuscript.

REFERENCES

Alford, R. M., 1986, Shear data in the presence of azimuthal anisotropy: 56th Ann. Internat. Mtg., Soc. Expl. Geophys., Expanded Abstract, 476–479.

Ata, E., and Michelena, R. J., 1995, Mapping distribution of fractures in a reservoir with *P-S* converted waves: The Leading Edge, **12**, 664–676.

Corrigan, D., Withers, R., Darnall, J., and Skopinski, T., 1996, Analysis of amplitude versus offset to detect gas-oil contacts in the Arabian Gulf: 66th Ann. Internat. Mtg., Soc. Expl. Geophys., Expanded Abstract, 1834–1837.

Garotta, R., and Granger, P. Y., 1988, Acquisition and processing of 3C × 3-D data using converted waves: 58th Ann. Internat. Mtg., Soc. Expl. Geophys., Expanded Abstract, 657–658.

Grechka, V., and Tsvankin, I., 1996, 3D description of normal moveout in anisotropic media: 66th Ann. Internat. Mtg., Soc. Expl. Geophys., Expanded Abstracts, 1487–1490.

Johnson, W. E., 1995, Direct detection of gas in pre-Tertiary sediments?: The Leading Edge, **14**, 119–122.

Lefeuvre, F., 1994, Fracture related anisotropy detection and analysis: "And if the *P*-waves were enough?": 64th Ann. Internat. Mtg., Soc. Expl. Geophys., Expanded Abstracts, 942–944.

Lynn, H., Simon, K. M., Layman, M., Schneider, R., Bates, C. R., and Jones, M., 1995, Use of anisotropy in *P*-wave and *S*-wave data for fracture characterization in a naturally fractured gas reservoir: The Leading Edge, **14**, 887–893.

Mallick, S., and Frazer, L. N., 1991, Reflection/transmission coefficients and azimuthal anisotropy in marine seismic studies: Geophys. J. Internat., **105**, 241–252.

Michelena, R. J., Ata, E., and Sierra, J., 1994, Exploiting *P-S* converted waves: Part 1, Modeling the effects of anisotropy and heterogeneities: 64 Ann. Internat. Mtg., Soc. Expl. Geophys., Expanded Abstract, 236–239.

Pérez, M., and Gibson, R., 1996, Detection of fracture orientation using azimuthal variation of *P*-wave AVO responses: Barinas Field (Venezuela): 66th Ann. Internat. Mtg., Soc. Expl. Geophys., Expanded Abstracts, 1353–1356.

Pérez, M., Gibson, R., and Töksoz, N., 1999, Detection of Fracture orientation from azimuthal variation of *P*-wave AVO responses: Geophysics, **64**, 1253–1267, this issue.

Rüger, A., 1996, Reflection coefficients and azimuthal AVO analysis in anisotropic media: Ph.D. thesis, Colorado School of Mines.